remote sensing

MDPI

Article

PRICOS: A Robust Paddy Rice Index Combining Optical and Synthetic Aperture Radar Features for Improved Mapping Efficiency

Yifeng Lou [1], Gang Yang [1,2,*], Weiwei Sun [1,2], Ke Huang [3], Jingfeng Huang [4], Lihua Wang [1,2] and Weiwei Liu [1]

[1] Department of Geography and Spatial Information Techniques, Ningbo University, Ningbo 315211, China; 2211420047@nbu.edu.cn (Y.L.); sunweiwei@nbu.edu.cn (W.S.); wanglihua1@nbu.edu.cn (L.W.); liuweiwei@nbu.edu.cn (W.L.)
[2] Zhejiang Collaborative Innovation Center for Land and Marine Spatial Utilization and Governance Research, Ningbo University, Ningbo 315211, China
[3] Faculty of Electrical Engineering and Computer Science, Ningbo University, Ningbo 315211, China; huangke599@gmail.com
[4] Institute of Applied Remote Sensing and Information Technology, Zhejiang University, Hangzhou 310058, China; hjf@zju.edu.cn
* Correspondence: yanggang@nbu.edu.cn

Abstract: Paddy rice mapping is critical for food security and environmental management, yet existing methods face challenges such as cloud obstruction in optical data and speckle noise in synthetic aperture radar (SAR). To address these limitations, this study introduces PRICOS, a novel paddy rice index that systematically combines time series Sentinel-2 optical features (NDVI for bare soil/peak growth, MNDWI for the submerged stages) and Sentinel-1 SAR backscatter (VH polarization for structural dynamics). PRICOS automates key phenological stage detection through harmonic fitting and dynamic thresholding, requiring only 10–20 samples per region to define rice growth cycles. Validated across six agroclimatic regions, PRICOS achieved overall accuracy (OA) and F1 scores of 0.90–0.98, outperforming existing indices like SPRI (OA: 0.79–0.95) and TWDTW (OA: 0.85–0.92). By integrating multi-sensor data with minimal sample dependency, PRICOS provides a robust, adaptable solution for large-scale paddy rice mapping, advancing precision agriculture and climate change mitigation efforts.

Keywords: paddy rice; sentinel series; time series; feature fusion; paddy rice index; SAR; optical data; PRICOS

check for updates

Academic Editor: Ruyin Cao

Received: 6 January 2025
Revised: 5 February 2025
Accepted: 13 February 2025
Published: 18 February 2025

Citation: Lou, Y.; Yang, G.; Sun, W.; Huang, K.; Huang, J.; Wang, L.; Liu, W. PRICOS: A Robust Paddy Rice Index Combining Optical and Synthetic Aperture Radar Features for Improved Mapping Efficiency. *Remote Sens.* **2025**, *17*, 692. https://doi.org/10.3390/rs17040692

Copyright: © 2025 by the authors. Licensee MDPI, Basel, Switzerland. This article is an open access article distributed under the terms and conditions of the Creative Commons Attribution (CC BY) license (https://creativecommons.org/licenses/by/4.0/).

1. Introduction

Rice, one of the most crucial staple crops globally, serves as a primary food source for billions of people [1,2]. However, rice cultivation is not only vital for food security but also resource-intensive, characterized by high irrigation water consumption and significant methane emissions resulting from anaerobic conditions in flooded paddies [3,4]. Therefore, monitoring the distribution and growth of paddy rice is essential for ensuring food security and sustainable agricultural practices, managing water resources, and mitigating environmental impacts [5,6]. Owing to the advancement of remote sensing technology, the efficient and rapid monitoring of the large-scale and long-term distribution of paddy rice planting areas has been achieved [7–9].

Currently, algorithms for mapping paddy rice planting areas using optical satellite data typically rely on the transplanting and heading phase characteristics captured by

multiple spectral indices [10]. These methods are known as phenology-based paddy rice mapping approaches and have been validated in various paddy rice-growing regions worldwide [11–13]. Specifically, vegetation indices, such as the Normalized Difference Vegetation Index (NDVI) and the Enhanced Vegetation Index (EVI), are commonly combined with water content indices, including the Land Surface Water Index (LSWI), the Normalized Difference Water Index (NDWI), and the Modified Normalized Difference Water Index (MNDWI) [10]. Among these indices, the condition where LSWI exceeds NDVI or EVI during the transplanting and heading period is considered to be the most classic [14]. However, the transplanting period is short, making it susceptible to weather conditions such as rain and snow, as well as the satellite's revisit cycle [3]. Moreover, when using the characteristics of the transplanting stage and the jointing stage, there is a relatively high similarity between paddy rice and wetland vegetation [15]. However, the accurate classification of multiple phenological periods requires abundant prior knowledge, which limits the large-scale application of this method [10].

SAR data have all-weather, all-day working observation and strong surface penetration capabilities, making them widely used for paddy rice mapping in low-latitude regions [16,17]. The scattering mechanism of SAR results in the low intensity of VH polarization for water bodies. Throughout the paddy rice cultivation cycle, a "V"-shaped pattern emerges in the VH time series. Utilizing this distinctive feature, early studies developed methods based on predefined thresholds [18–20]. Although these methods are simple and efficient, the problem is that VH intensity in rice can be affected by factors such as topography, environmental conditions, and incident angle, resulting in different time series characteristics across regions [21,22]. Consequently, specific thresholds are unsuitable for large-scale paddy rice mapping. To address this issue, Xu et al. (2023) proposed a SAR-based paddy rice index (SPRI) that adjusts the vegetation reference value (v) and water reference value (w) to enhance performance in various regions [10]. However, SAR backscatter signals are prone to noise interference, resulting in "salt-and-pepper" effects that can degrade the land cover classification performance [23,24].

To address the limitations of single-source data, fusing SAR and optical data can reduce the noise in SAR data and compensate for gaps in the optical data caused by cloud cover and rainfall [25–30]. Currently, many studies use feature fusion approaches that directly incorporate both optical and SAR features into machine learning or deep learning models for improved mapping results [31,32]. For example, Chen et al. (2020) fused Sentinel-1 and Sentinel-2 polarization data with spectral indices, applying the random forest (RF) algorithm to paddy rice mapping in China's Jianghan Plain [33]. The results indicated that the mapping accuracy significantly improved with the inclusion of SAR data. However, these methods require large training datasets to achieve high accuracy. The process of gathering sample data is time-consuming, labor-intensive, and financially costly, thereby limiting its practicality in large-scale crop mapping [34,35].

To address these challenges, especially those related to feature extraction design for paddy rice identification using vegetation indices and the use of manual threshold methods or relatively complex parameter designs in the SAR data, this study combines Sentinel-1 and Sentinel-2 time series data to automatically detect key phenological stage information and to develop the Paddy Rice Index Combining Optical and SAR features (PRICOS). The specific objectives of this study are as follows: (1) By integrating the advantages of both optical and SAR data, the method ensures its universality across multiple regions and its applicability to large-scale areas by automatically extracting the key phenological features of paddy rice. (2) By simplifying the parameter selection process and adopting more robust algorithms, the method ensures the stability of the threshold range.

2. Materials

2.1. Study Area

This study explored the diversity of paddy rice cultivation patterns and selected six study sites based on available ground reference data. These sites feature varying climatic, topographical, and landscape conditions. Among them, three sites in China (Sites A–C) were designated as method development areas, while the sites in Vietnam (Site D), Japan (Site E), and the United States (Site F) were designated as method transfer areas (Figure 1).

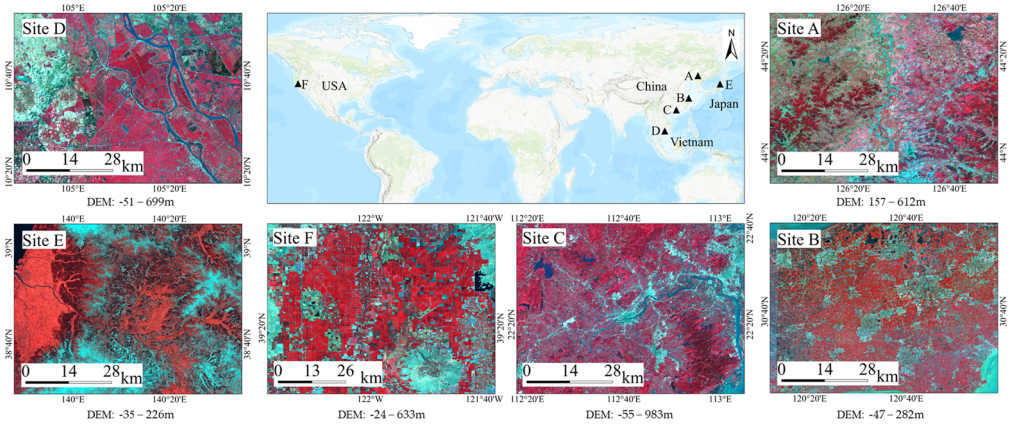


Figure 1. Geographical locations of the study area and the Sentinel-2 median composite images (RGB: B8-B4-B3). The triangles indicate the specific locations of the study sites. Site A is in Shulan City, Jilin Province; Site B is in the Hangjiahu Plain, Zhejiang Province; Site C is in Guangzhou, Guangdong Province; Site D is in Can Tho City, Vietnam; Site E is in Aomori Prefecture, Japan; and Site F is in California, the USA.

Site A (126.05–126.85°E, 43.9–44.5°N), located in Shulan City, Jilin Province, China, is predominantly flat with a temperate monsoon climate. The average annual temperature is 4.6 °C, and the annual precipitation is 650 mm. This area belongs to the single-season rice region, where rice is transplanted in mid-May and harvested in early October.

Site B (120.2–121°E, 30.3–30.9°N), located in Zhejiang Province, mainly covers the Hangjiahu Plain, a key paddy rice production region. This region has a subtropical monsoon climate, with an average annual temperature of 16.6 °C and an annual precipitation of 1450 mm. The region experiences a plum rain season during the spring and summer. This area supports a double-cropping system, with rice transplantation occurring in mid-June and harvesting taking place in early November.

Site C (112.3–113.1°E, 22.1–22.7°N), located in Guangzhou, Guangdong Province, China, features hilly terrain and a marine subtropical monsoon climate. The average annual temperature is 21.8 °C, with substantial rainfall averaging 1900 mm annually. The area supports double or triple cropping, with early rice transplanted in mid-March and harvested in late July, and late rice transplanted from late July to early August and harvested in early December.

Site D (104.8–105.6°E, 10.3–10.9°N), located in Can Tho City, southern Vietnam, features flat terrain and a tropical monsoon climate. The average annual temperature is 25.5 °C, and the annual precipitation is 1600 mm, ideal for the double or triple cropping of paddy rice. Early rice is typically transplanted from mid-March to early April and harvested in early July, while late rice is transplanted from late July to early August and harvested from late November to December.

Site E (139.8–140.6°E, 38.5–39.1°N), located in Aomori Prefecture, Japan, features hilly terrain and a temperate oceanic climate. The average annual temperature is around 10 °C,

with an annual precipitation of 1200 mm. Paddy rice is planted once a year, transplanted from mid-May to early June, and harvested in September.

Site F (121.61–122.31°W, 39.15–39.65°N), located in California, USA, is a flat area with a Mediterranean climate. It has an average annual temperature of 12 °C and an annual precipitation of 500 mm. Paddy rice is transplanted in May and harvested in September or October.

2.2. Satellite Data

The Sentinel-1 satellites, with their synthetic aperture radar (SAR) sensors, operate in a dual-satellite configuration. The two satellites have a revisit period of about six days. This dual-satellite setup allows for more comprehensive monitoring of various aspects such as land cover, glaciers and ice caps, oceans, and disasters. The dual-satellite system provides enhanced capabilities for data collection and coverage, enabling more detailed and accurate mapping of the Earth's surface, and ensuring continuous monitoring over a wide range of areas. Sentinel-2 is equipped with a Multispectral Instrument (MSI) that has a revisit period of five days and is widely used for land cover classification, vegetation monitoring, and agricultural assessments. The open accessibility, high quality, and comprehensive global coverage of Sentinel data render them an indispensable resource for earth science research, natural resource management, and environmental monitoring.

In this study, all available Sentinel-1 Ground Range Detected (GRD) products and Sentinel-2 Level-1C products for the target years covering the study areas were accessed via the Google Earth Engine (GEE) platform. For the SAR data, the Lee-sigma filter was applied to suppress speckle noise, using a filter window size of 5. For the Sentinel-2 data, the Quality Assurance (QA) band was utilized for cloud masking.

2.3. Validation Data

The sample dataset for the Chinese sites was obtained through field surveys that integrated GPS points with UAV imagery, totaling 6687 sample points. Specifically, Site A included samples of paddy rice, corn, soybean, peanuts, forests, water bodies, bare land, and built-up areas. Samples from Sites B and C were classified into two categories: paddy rice and non-paddy rice. This dataset was developed by Professor Yuan Wenping's team at Sun Yat-sen University. The sample datasets for Vietnam and Japan were randomly generated using high-resolution land use and land cover data (JHR-LULC) (https://www.eorc.jaxa.jp/ALOS/en/lulc/data/index.htm, accessed on 10 October 2024, 10 m), categorized into paddy rice and non-paddy rice classes. Vietnam had a total of 903 sample points, while Japan had a total of 937 sample points. This dataset was produced by the Japan Aerospace Exploration Agency (JAXA). The sample dataset for the United States was randomly generated based on the U.S. Department of Agriculture's Cropland Data Layer (USA-CDL) (https://nassgeodata.gmu.edu/CropScape/, accessed on 20 September 2024, 30 m) [36], and also categorized into paddy rice and non-paddy rice classes, with a total of 1000 sample points.

For validation, this study selected paddy rice products from the 2017–2022 Chinese high-resolution single-season paddy rice dataset (10m) [37], the Chinese double-cropping paddy rice dataset (2016–2020) [38], JHR-LULC, and USA-CDL. These datasets were compared with the PRICOS extraction results for Site A (2019), Site B (2018), Site C (2019), Site D (2020), Site E (2022), and Site F (2019) to further validate the accuracy of the results.

3. Method

This study developed a novel method for mapping paddy rice, named PRICOS. The method included the following steps (Figure 2): (1) Time series Sentinel-1/2 data were

obtained through the Google Earth Engine (GEE) platform and preprocessed. (2) The paddy rice growing cycle was established by comparing the time series NDVI, MNDWI, and VH values of the paddy rice samples. (3) The maximum and minimum values of time series NDVI, the maximum value of time series MNDWI, and the maximum and minimum values of time series VH were automatically extracted during the paddy rice growing period. (4) Phenological significance was assigned to the maximum and minimum values, and the data were re-quantified accordingly. (5) PRICOS was calculated, and index thresholds were established using validation samples to generate the paddy rice distribution map.

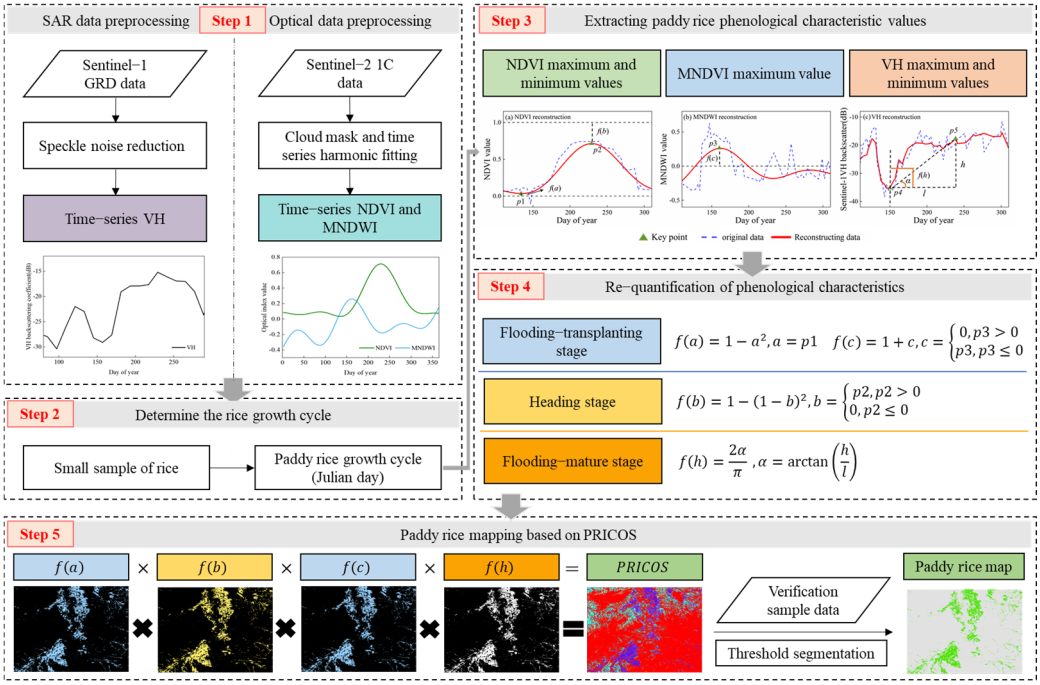


Figure 2. The workflow of PRICOS for mapping paddy rice.

3.1. Time Series Feature Analysis

Paddy rice typically goes through four stages: transplanting, growth, maturation, and harvest [39]. Before transplanting, agricultural activities such as plowing and field flooding are carried out. After transplanting, as paddy rice grows, it will exhibit obvious vegetation characteristics at the peak of growth. In the time series, paddy rice shows a distinct pattern of bare soil, water bodies, and vegetation.

In terms of optical data, the Normalized Difference Vegetation Index (NDVI) time series can effectively monitor the growth of vegetation and distinguish between bare soil and vegetation, providing a valuable reference for differentiating crops from other land cover types. The Modified Normalized Difference Water Index (MNDWI) can identify the features of water bodies. Combining NDVI with MNDWI enables the extraction of two key features, namely water bodies and vegetation, which helps to distinguish paddy rice from other crops.

In the synthetic aperture radar (SAR) data, during the submerged-transplanting stage, the surface of the paddy field is mainly water or moist and smooth soil, and surface scattering predominates at this time (resulting in lower dB values). At the peak growth stage, paddy rice plants reach their maximum height and form a closed canopy, which will reduce surface scattering and introduce double-bounce scattering components (resulting in higher dB values). From the submerged-transplanting stage to the peak growth stage, the total backscatter intensity of the paddy field increases continuously with significant variations. Previous studies have shown that compared with Vertical–Vertical (VV) po-

larization, Vertical–Horizontal (VH) polarization can provide more accurate classification results for paddy rice crops [39,40]. Therefore, this study calculated the NDVI and MNDWI time series using the Sentinel-2 data and combined them with the VH backscatter time series from the Sentinel-1 data. Utilizing the eight land cover types in Site A, we illustrated the NDVI time series (Figure 3a), MNDWI time series (Figure 3b), and VH time series (Figure 3c). In Figure 3a, the NDVI values for crops between 130 and 170 days are relatively low, resembling those of bare soil and built-up areas. The NDVI values between 200 and 250 days are higher, resembling those of forested areas. Combining these two features allows for the effective separation of crops from forests, water bodies, and built-up areas. In Figure 3b, the MNDWI values for paddy rice between 130 and 160 days are higher, similar to those of water bodies, while the values during other periods resemble those of other land covers, demonstrating a distinctive "water-other" pattern. The combination of NDVI and MNDWI enables the complete identification of paddy rice's unique growth characteristics, specifically the bare soil–water body–vegetation pattern. In Figure 3c, the backscatter intensity of paddy rice between 140 and 160 days is similar to that of water bodies but lower than that of other land covers. However, between 260 and 270 days, the backscatter intensity of paddy rice is slightly lower than that of built-up areas and vegetation, resembling that of other crops. In summary, the integration of optical and SAR data enhances and enriches the unique characteristics of paddy rice. The calculation formulae for NDVI and MNDWI are as follows:

$$NDVI = \frac{NIR - Red}{NIR + Red} \tag{1}$$

$$MNDWI = \frac{Green - SWIR1}{Green + SWIR1} \tag{2}$$

where NIR, Red, $Green$, and $SWIR1$ are the reflectance values of bands B8, B4, B3, and B11 in Sentinel-2.

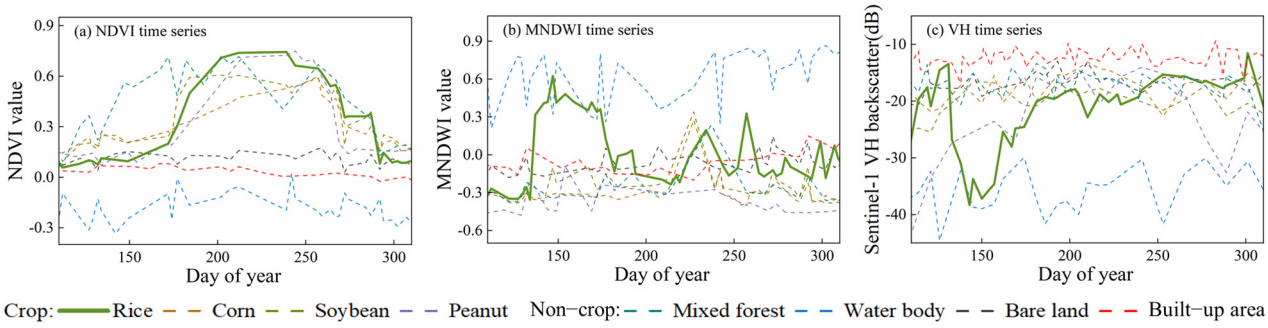


Figure 3. Time series characteristics of eight types of land objects.

After cloud masking, the Sentinel-2 imagery exhibits numerous missing values within the original time series. Given that the NDVI and MNDWI time series describe the phenological characteristics of paddy rice, this study reconstructs the time series using harmonic fitting to capture the periodic characteristics (Figure 4a,b). Based on the cropping systems of the four sites, the fitting frequency was set to 3 (refer to Section 5.1 for details). The fitting formula is as follows:

$$\hat{p}(t) = a + bt + \Sigma_{n=1}^{3}\left(c_n cos\left(\frac{2\pi n}{T}\right) + d_n sin\left(\frac{2\pi n}{T}\right)\right) \tag{3}$$

where $\hat{p}(t)$ is the fitting value on day t, t is the Julian day, a is the overall horizontal offset value, b is the linear coefficient, c_n and d_n are the coefficients of sine and cosine functions with different frequencies, and T is the number of days in a year.

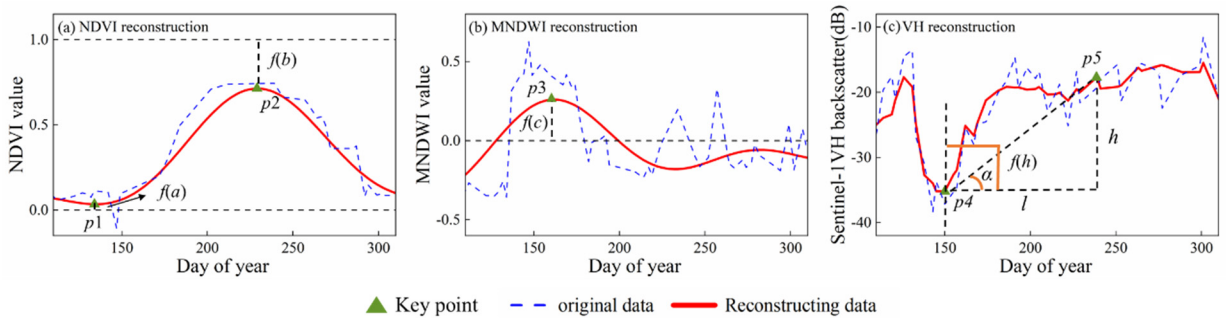


Figure 4. Reconstruction of time series for NDVI, MNDWI, VH, and the design of rice index features.

3.2. PRICOS Construction

As shown in Figure 4a, in the Normalized Difference Vegetation Index (NDVI) time series, the pixels of the paddy field exhibit a "valley" shape between the 130th and 160th days (transplanting stage), and its minimum value (p1) is close to 0. According to Equation (4), f(a) quantifies the distance between p1 and 0. Squaring a will amplify the difference from evergreen vegetation, and its value range is from 0 to 1. During the jointing stage (from the 220th to 240th days), a "peak" shape appears, and the maximum value (p2) is close to 1. According to Equation (5), f(b) quantifies the distance between p2 and 1. If p2 is less than or equal to 0, the result is 0; if p2 is greater than 0, then (1—b) is squared to amplify the difference from non-vegetation, and its value range is from 0 to 1.

As illustrated in Figure 4b, the Modified Normalized Difference Water Index (MNDWI) time series indicates that the pixels of the paddy field exhibit water body characteristics between the 140th and 160th days (submerged-transplanting stage), and its value (p3) is close to that of the water bodies. At this time, the MNDWI value is usually greater than or equal to 0. According to Equation (6), f(c) quantifies the distance between p3 and 0. If p3 is greater than 0, it will be identified as a water body or a background with a significant water body presence, and the result will be 1. If p3 is less than or equal to 0, considering the data quality or the fitting smoothing effects, values closer to 0 are more likely to indicate the presence of water. Its value range is also from 0 to 1.

As shown in Figure 4c, the Vertical–Horizontal (VH) time series shows that the pixels of the paddy field reach a minimum value (p4) on the 146th day (transplanting stage), and we choose the maximum value within the jointing stage (from the 220th to 240th days) as p5. According to Equation (7), f(h) quantifies the difference between p4 and p5 (denoted as h). In order to standardize the range of the calculation results, the time difference l between p4 and p5 is divided by 30, and then the difference h is converted into an angle α using a trigonometric function. Relative to a right angle, its value range is from -1 to 1. The closer the calculated value is to 1, the higher the probability that the pixel represents paddy rice. Moreover, paddy rice must satisfy these four features simultaneously. Therefore, these four feature values are combined multiplicatively. The specific formula is as follows:

$$f(a) = 1 - p1^2 \tag{4}$$

$$f(b) = 1 - (1 - p2)^2,\ p2 > 0,\ f(b) = 0,\ p2 \le 0 \tag{5}$$

$$f(c) = 1 + p3,\ p3 \le 0,\ f(c) = 0,\ p3 > 0 \tag{6}$$

$$f(h) = \frac{2\alpha}{\pi},\ \alpha = arctan\left(\frac{30h}{l}\right) \tag{7}$$

The formula for the paddy rice index is as follows:

$$PRICOS = f(a) \times f(b) \times f(c) \times f(h) \tag{8}$$

The formula of the index constructed using optical conditions is as follows:

$$OPRI = f(a) \times f(b) \times f(c) \tag{9}$$

3.3. Performance Evaluation

In this study, we assessed the accuracy of paddy rice mapping using sample data by calculating the producer's accuracy (PA), user's accuracy (UA), overall accuracy (OA), and F1 score from the confusion matrix of the validation samples. The calculation formulae are as follows:

$$PA = \frac{TP}{TP + FN} \tag{10}$$

$$UA = \frac{TP}{TP + FP} \tag{11}$$

$$OA = \frac{TP + TN}{TP + TN + FP + FN} \tag{12}$$

$$F1\ score = \frac{2 \times UA \times PA}{UA + PA} \tag{13}$$

where TP refers to the number of correctly classified paddy rice samples, TN refers to the number of correctly classified non-paddy rice samples, FP refers to the number of non-paddy rice samples incorrectly classified as paddy rice, and FN refers to the number of paddy rice samples incorrectly classified as non-paddy rice.

The applicability of PRICOS was further assessed by comparing it with the optical paddy rice index (OPRI), SPRI, FARM, and a paddy rice dataset generated using the Time-Weighted Dynamic Time Warping (TWDTW) method. OPRI is the optical paddy rice index developed in this study using Sentinel-2 time series data (see Equation (9)). SPRI is a novel object-based paddy rice index derived from SAR time series data. In the mapping of Sites A to F, the value of v is set at the 25th percentile, while the w values are selected from the 25th, 90th, 90th, 50th, and 25th percentiles. Segmentation is performed using the highest accuracy threshold determined from the sample evaluation in this study to generate the final paddy rice map. FARM is a fully automated paddy rice mapping framework that integrates Sentinel-1 SAR and Sentinel-2 multi-temporal images. In FARM mapping, each study site is trained with 2000 automatically generated sample points for both paddy rice and non-paddy rice. All methods were assessed for accuracy using the samples collected in this study.

4. Results

4.1. PRICOS Threshold for Rice Planting Area Mapping

Using PRICOS, we generated paddy rice planting probability distribution maps for Sites A to C. By combining visual inspection with sample statistics, the results from the OSPRI calculation indicate a clear distinction between paddy rice and non-paddy rice pixels, allowing the same threshold to be used for segmentation. Specifically, as shown in Figure 5, after the OSPRI calculation, the pixel values representing paddy rice features are higher (blue), while the pixels for other crops are intermediate (green or light blue), and those for forests, water bodies, and built-up areas are lower (red or orange), demonstrating a clear distinction. We classified the sample points for Sites A to C into paddy rice and other land cover types and conducted a comprehensive statistical analysis of the OSPRI values for both categories across the three sites. The statistical results (Figure 6) suggest that a threshold of 0.6 can be applied across all three sites.

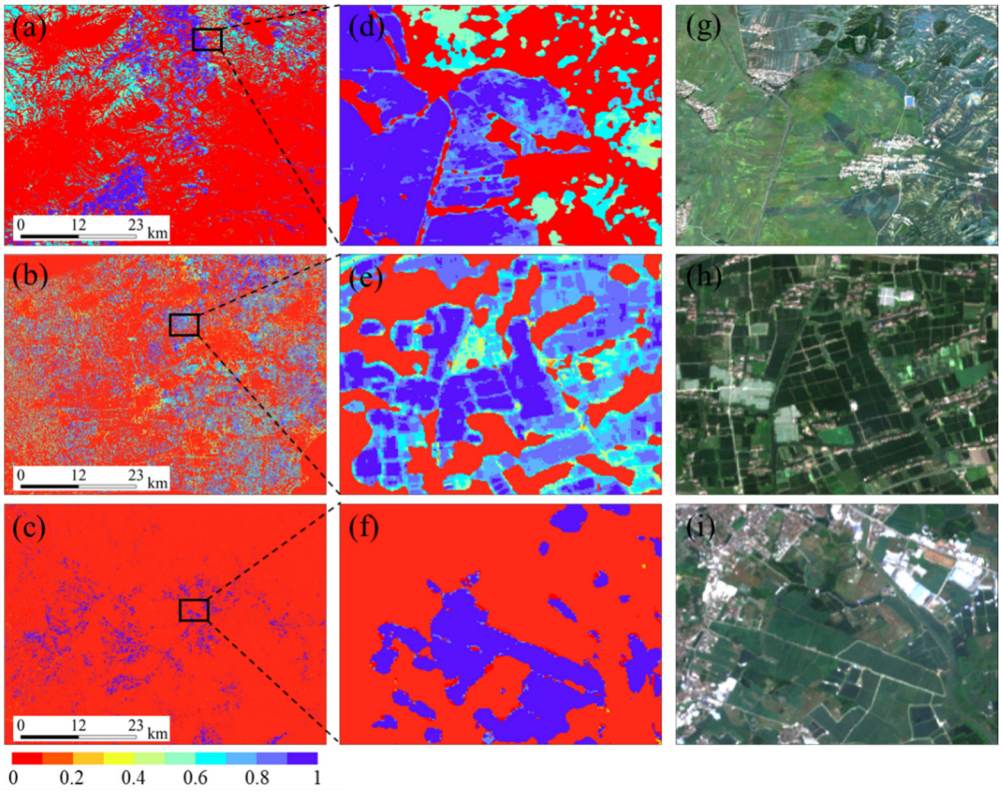


Figure 5. PRICOS values and zoomed-in views. The first column (**a**–**c**) displays the OSPRI calculation results for Sites A to C. The second column (**d**–**f**) provides a zoomed-in view. The third column (**g**–**i**) displays the Sentinel-2 RGB image corresponding to the zoomed-in view.

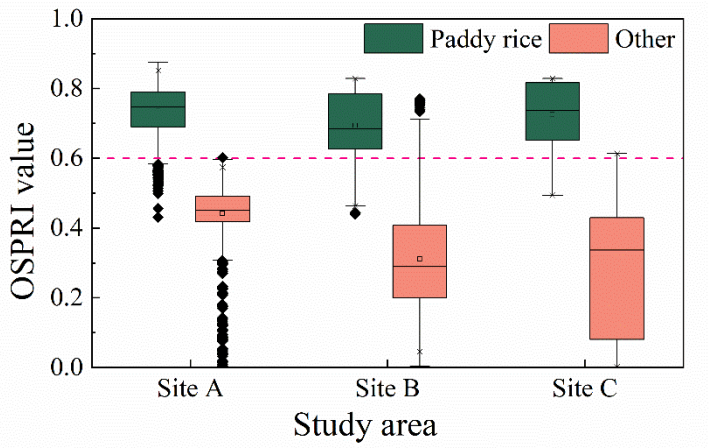


Figure 6. PRICOS values for five land cover types.

4.2. Accuracy Assessment

Table 1 presents the results of UA, PA, OA, and F1 for Sites A to F. The results show OA and F1 scores above 0.90, with UA being greater than 0.90 and PA above 0.91. Specifically (Figure 7), at Site A, rice planting was concentrated in large patches along rivers, with an OA of 0.97 and F1 score of 0.97, closely matching the Sentinel-2 imagery. At Site B, fragmented rice fields around built-up areas had an OA of 0.91 and F1 score of 0.93, showing good agreement despite the smaller field patches. Site C had rice distributed in valleys and along riverbanks, with smaller fields and somewhat blurred boundaries, achieving an OA of 0.97 and F1 score of 0.96. At Site D, the mapping results matched the satellite imagery well, with a high UA, indicating most rice areas were correctly identified. Site E, affected by cloud cover, used composite images from April to May and showed a high accuracy with an OA

of 0.95 and F1 score of 0.96. Site F showed regular-shaped rice fields, achieving an OA of 0.98 and F1 score of 0.98, demonstrating high consistency with the reference maps. These results show that PRICOS, with a 0.6 threshold, provides accurate and reliable paddy rice maps across diverse locations.

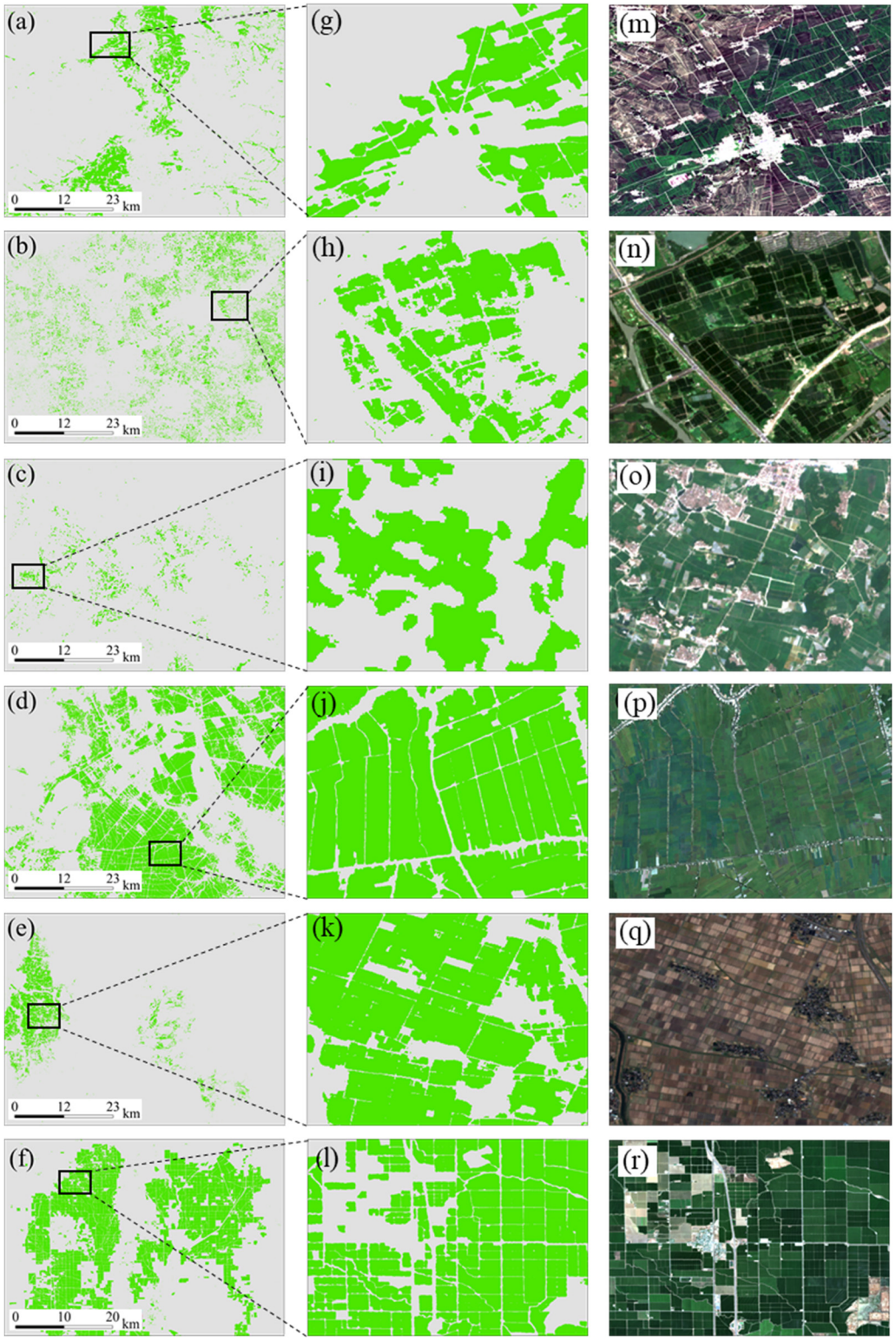


Figure 7. Rice extraction results from six sites. The first column (**a**–**f**) displays the rice mapping results based on PRICOS for Sites A to F. The second column (**g**–**l**) provides an enlarged view. The third column (**m**–**r**) displays the Sentinel-2 RGB image corresponding to the enlarged view.

Table 1. Accuracy assessment of rice mapping methods and datasets (r: rice; nr: non-rice).

Study Area	Sample Size (r/nr)	Methods/Dataset	UA	PA	OA	F1
Site A	2276/2307	PRICOS	0.99	0.95	0.97	0.97
		OPRI	0.96	0.95	0.96	0.95
		SPRI	0.90	0.78	0.84	0.81
		FARM	1.00	0.88	0.94	0.95
		TWDTW	0.99	0.85	0.92	0.91
Site B	962/630	PRICOS	0.93	0.93	0.92	0.93
		OPRI	0.76	0.79	0.78	0.77
		SPRI	0.80	0.80	0.80	0.80
		FARM	0.88	0.85	0.87	0.86
		TWDTW	0.87	0.82	0.85	0.84
Site C	222/290	PRICOS	0.98	0.94	0.96	0.96
		OPRI	0.97	0.82	0.90	0.90
		SPRI	0.94	0.93	0.94	0.94
		FARM	0.98	0.95	0.96	0.96
		TWDTW	0.98	0.78	0.88	0.88
Site D	439/464	PRICOS	0.90	0.91	0.90	0.90
		OPRI	0.88	0.82	0.86	0.85
		SPRI	0.84	0.73	0.79	0.78
		FARM	0.95	0.93	0.94	0.94
Site E	551/386	PRICOS	0.96	0.97	0.95	0.96
		OPRI	0.97	0.82	0.90	0.90
		SPRI	0.97	0.72	0.83	0.83
		FARM	0.93	0.94	0.94	0.93
Site F	500/500	PRICOS	0.99	0.96	0.98	0.98
		OPRI	0.96	0.96	0.96	0.96
		SPRI	0.96	0.93	0.95	0.95
		FARM	0.99	0.97	0.98	0.98

4.3. Visual Comparison with Other Methods

At six sites, we evaluated PRICOS through visual assessments and quantitative sample evaluations, comparing it with other methods (Figure 8). Overall, PRICOS demonstrated a high similarity to the reference maps and Sentinel-2 imagery, with balanced omission and commission errors, achieving moderate to high OA and F1 scores.

At the three sites in China, PRICOS outperformed the other methods. At Site A in Northeast China, PRICOS achieved the highest OA and F1 scores, showing a high consistency with satellite imagery. At Site B in East China, PRICOS showed good accuracy with an OA of 0.92 and F1 score of 0.93, despite some boundary omissions. Site C in South China showed slightly higher commission errors for PRICOS compared to FARM, but its OA (0.96) and F1 score (0.96) were still competitive.

In Vietnam (Site D) and Japan (Site E), where field data were unavailable, JHR-LULC served as the reference map. At Site D, PRICOS maintained an OA above 0.90, despite identifying fewer paddy rice targets than FARM. At Site E, PRICOS achieved the highest similarity to JHR-LULC, with OA and F1 scores of 0.95 and 0.96, respectively. At Site F in the United States, all methods performed well, with PRICOS and FARM achieving an OA and F1 score of 0.98, closely matching the USA-CDL reference.

Overall, PRICOS provided reliable and accurate paddy rice mapping across diverse geographic locations.

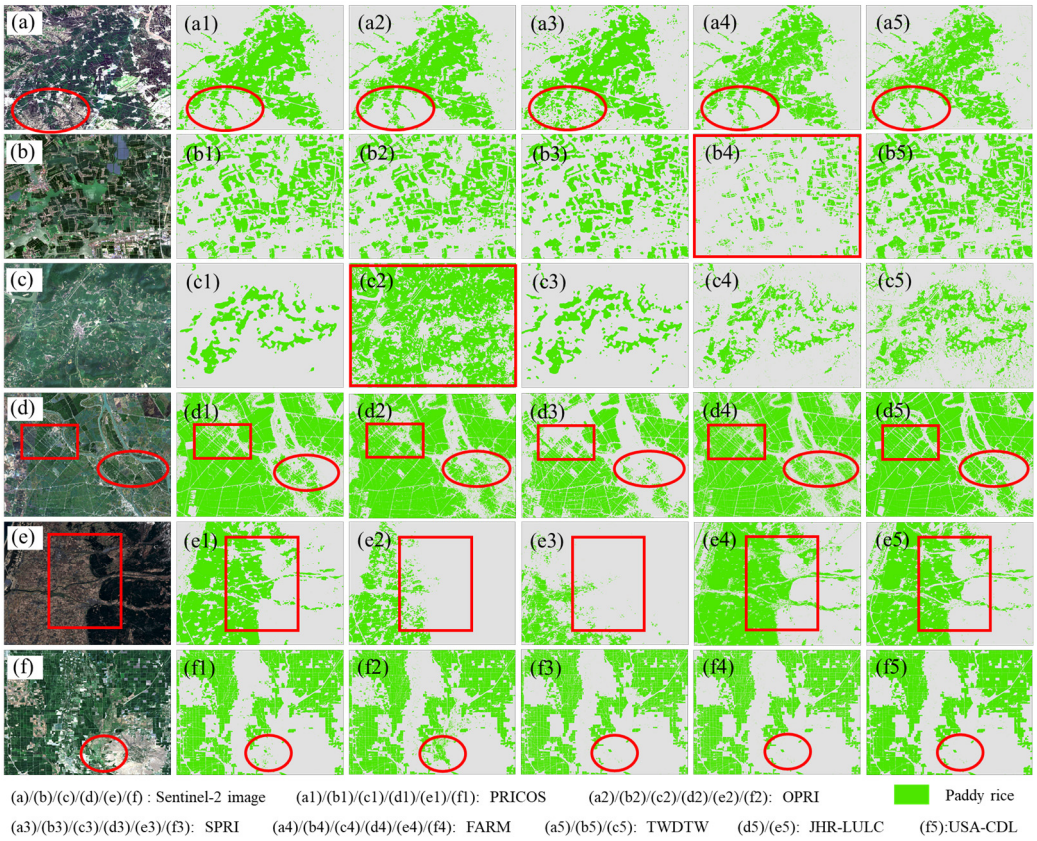


Figure 8. Comparison with other methods and data products. The red ellipses and rectangles indicate areas with significant differences. (The red rectangle and ellipse highlight areas with significant differences).

5. Discussion

5.1. Harmonic Fitting Period Analysis

In this study, PRICOS utilizes four key features, three of which are derived from optical data through harmonic fitting. This reconstruction method is critical for PRICOS's performance as it captures the phenological patterns necessary to differentiate paddy rice from other land cover types. Our analysis of different harmonic fitting frequencies (1, 2, 3, and 4) across three sites (A, B, and C) provides insights into how the fitting frequency affects model performance.

As shown in Figure 9, when the fitting frequency was set to 1, the data at Site A adequately represented the phenology of paddy rice. However, at Sites B and C, the data appeared overly smoothed and failed to capture the nuanced phenological characteristics. Increasing the fitting frequency to 2, 3, and 4 significantly improved the reconstruction accuracy, with the frequencies of 3 and 4 being the most effective in capturing the actual phenological trends.

When evaluating PRICOS's performance using the F1 score (Figure 10), we observed that the highest accuracy was achieved with a fitting frequency of 3. This finding aligns with previous studies [41], which found that selecting an optimal harmonic frequency is essential to balance model sensitivity and avoid overfitting, especially in regions with diverse phenological stages.

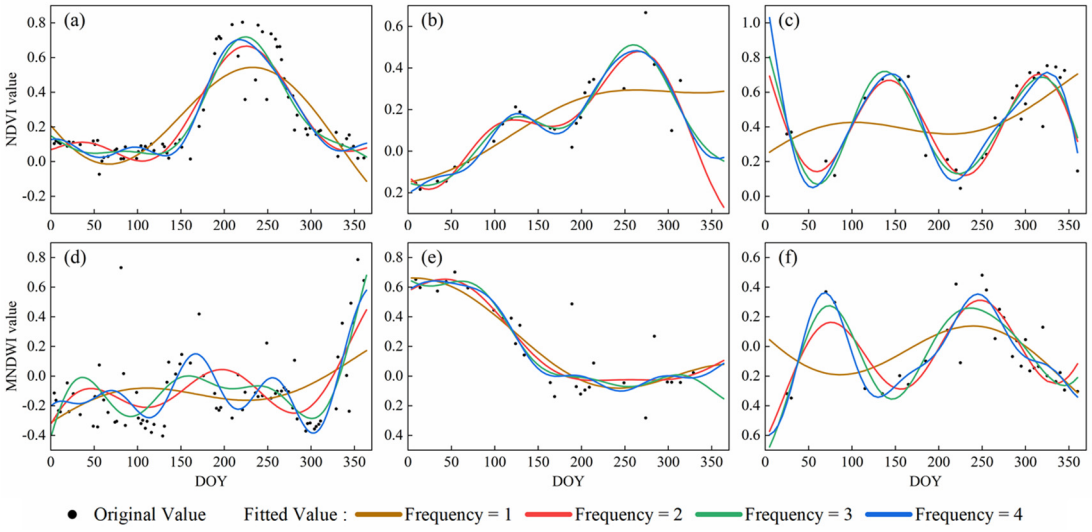


Figure 9. Optical index fitting results at different harmonic frequencies. (**a**–**c**) are the raw NDVI values with different frequency fits for sites A, B, and C, respectively. (**d**–**f**) are the raw MNDWI values with different frequency fits for sites A, B, and C, respectively.

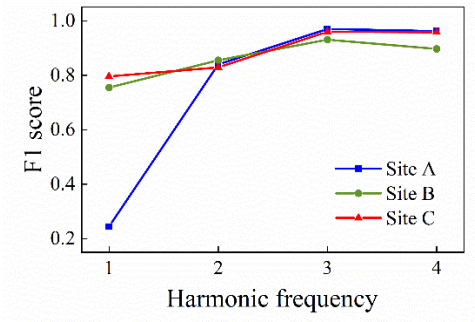


Figure 10. Analysis of PRICOS mapping accuracy at different harmonic fitting frequencies.

5.2. Feature Contribution Analysis

PRICOS integrates three optical features and one SAR feature to distinguish paddy rice from non-paddy rice. As shown in Figure 11, The optical features based on NDVI (f(a) and f(b)) effectively separate crops from non-crops, while the MNDWI-based feature (f(c)) helps distinguish water bodies from non-water bodies. The SAR-based feature (f(h)) provides additional structural information, which is crucial for improving paddy rice identification.

Using ground truth samples from Site A, we analyzed the contribution of various feature combinations (f(a) × f(b), f(c), and f(a) × f(b) × f(c)). The results indicated that f(a) × f(b) effectively separated crops from non-crops, with a clear distinction between the two categories. The combination of NDVI and MNDWI (f(a) × f(b) × f(c)) further enhanced the ability to distinguish paddy rice from other crops, emphasizing the importance of using both optical indices.

The analysis of f(h) revealed challenges due to the variability in h values across different terrain types, paddy rice varieties, cultivation methods, and incident angles. As shown in Figure 12a, Sites A and C exhibited relatively distinct h value distributions for paddy rice and non-paddy rice. This indicates that SAR data can provide additional structural information to improve paddy rice identification. However, Site B presented more overlaps between the two categories, suggesting that SAR features may perform differently in regions with more heterogeneous cropping practices. This finding corroborates previous studies [10], which highlighted that the sensitivity of SAR data to terrain and crop variability could lead to challenges in heterogeneous regions.

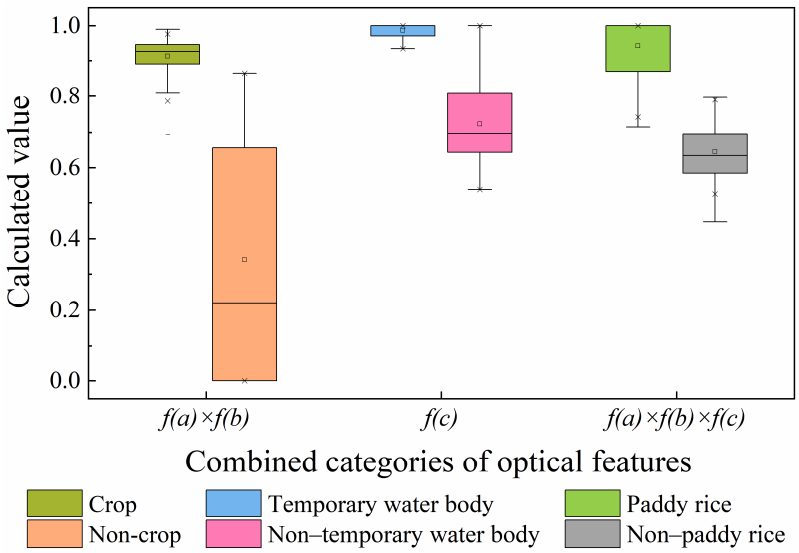


Figure 11. Calculated values for three different combinations of optical features.

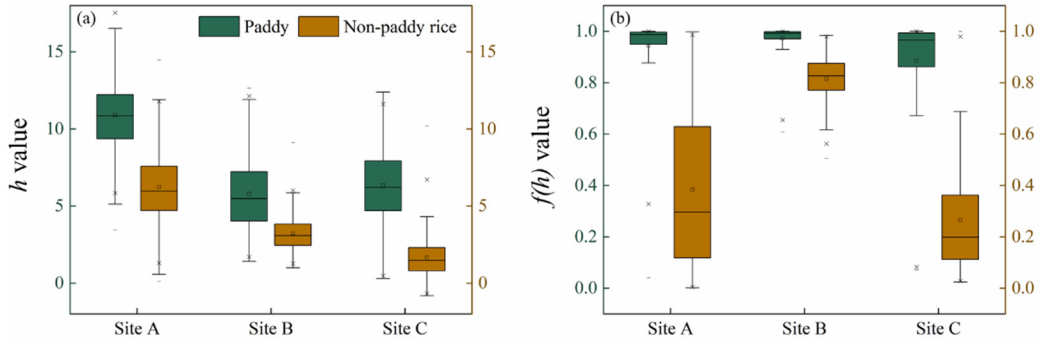


Figure 12. (**a**,**b**) are the h and f(h) values of rice and non-rice samples in locations A–C, respectively. The left axis represents the distribution of h values and f(h) values for paddy rice samples, while the right axis represents the distribution of h values and f(h) values for non-paddy rice samples.

5.3. Advantages and Limitations

PRICOS provides several advantages over conventional mapping methods. First, the integration of both optical and SAR data enhances the accuracy and reliability of paddy rice mapping, particularly in areas with frequent cloud cover or complex terrain. Previous research has demonstrated that combining multi-source data improves the robustness and consistency of crop mapping in challenging environments, such as regions with diverse topography or frequent cloud cover [42,43].

Second, PRICOS requires minimal training data (only 10 to 20 paddy rice samples per site), making it more efficient than machine learning-based methods, which typically require extensive labeled datasets. Our results (Figure 10) show that PRICOS achieves a high accuracy with limited data, making it ideal for large-scale mapping applications.

However, PRICOS has some limitations. The reliance on a fixed combination of optical and SAR features means that the model's performance is heavily dependent on the validity of these features in the region being mapped. In areas with significant terrain variation or altered phenological cycles, such as mountainous regions or areas affected by climate change, PRICOS may face difficulties in accurately identifying paddy rice. This was observed at Site B, where the separation between paddy rice and non-paddy rice was less distinct.

To address these limitations, future work will focus on developing a more adaptive framework that can automatically adjust feature combinations based on data conditions

and regional characteristics. This could involve integrating machine learning techniques to refine the feature set based on local data, as well as optimizing thresholds dynamically to improve the performance in challenging environments.

In conclusion, while PRICOS demonstrates robust performance in regions with typical phenological cycles and terrain, there is a need for further development to enhance its adaptability to regions with atypical agricultural practices or challenging environmental conditions. Future versions of PRICOS will prioritize the integration of adaptive mechanisms to improve its generalization across diverse regions, while maintaining the computational efficiency that makes PRICOS suitable for large-scale applications.

6. Conclusions

This study developed PRICOS, a novel paddy rice mapping framework that synergizes time series optical and SAR data to address the limitations of conventional vegetation index-based methods. Unlike traditional approaches that rely on single-source optical indices or predefined thresholds for phenological stages, PRICOS integrates multi-temporal spectral and structural features to systematically capture the full growth cycle of paddy rice. Key advancements and findings include the following: (1) PRICOS combines NDVI, MNDWI, and VH backscatter to overcome the data gaps in optical methods and the noise limitations in SAR-only approaches. This fusion achieved OA and F1 scores of 0.90–0.98 across seven regions, outperforming standalone indices like SPRI (OA: 0.79–0.95) and TWDTW (OA: 0.85–0.92). Compared to classical water–vegetation transition indices, PRICOS reduces the misclassification of wetlands and non-rice crops by leveraging SAR-derived structural consistencies. (2) By harmonizing Sentinel-1/2 time series data and applying harmonic fitting, PRICOS automates the identification of critical growth stages without manual threshold tuning. This contrasts with rule-based methods that require region-specific prior knowledge. (3) Validated across diverse climates, terrains, and cropping systems, PRICOS demonstrates a consistent performance with fixed thresholds (0.6) and minimal samples. This scalability addresses the labor-intensive sample collection required by index-based workflows. While PRICOS advances optical–SAR integration, its reliance on harmonic fitting for optical data reconstruction remains a limitation in persistently cloudy regions. Future work will prioritize SAR-centric adaptations to further reduce optical dependencies. Overall, PRICOS bridges the gap between oversimplified vegetation indices and complex multi-sensor models, providing a robust, efficient solution for global paddy rice monitoring.

Author Contributions: Conceptualization, Y.L. and K.H.; methodology, Y.L., G.Y., J.H. and W.S.; software, Y.L.; validation, Y.L. and G.Y.; formal analysis, G.Y. and L.W.; investigation, Y.L. and W.L.; resources, Y.L. and G.Y.; data curation, Y.L. and G.Y.; writing—original draft preparation, Y.L. and G.Y.; writing—review and editing, Y.L., G.Y., K.H. and J.H.; visualization, Y.L. and G.Y.; supervision, J.H.; funding acquisition, G.Y., J.H., L.W. and W.L. All authors have read and agreed to the published version of the manuscript.

Funding: This research was funded by the National Natural Science Foundation of China (Grant No. 42171314, 42271340), and the Public Projects of Ningbo City (Grant No. 2023S102, 2023S118).

Data Availability Statement: Data are available from the corresponding authors upon request.

Conflicts of Interest: The authors declare that they have no known competing financial interests or personal relationships that could have appeared to influence the work reported in this paper.

References

1. Elert, E. Rice by the numbers: A good grain. *Nature* **2014**, *514*, S50. [CrossRef] [PubMed]
2. FAO. *World Food and Agriculture Statistical Yearbook 2022*; FAO: Rome, Italy, 2022. [CrossRef]

3. Dong, J.; Xiao, X. Evolution of regional to global paddy rice mapping methods: A review. *ISPRS J. Photogramm. Remote Sens.* **2016**, *119*, 214–227. [CrossRef]
4. Zhang, B.; Tian, H.; Ren, W.; Tao, B.; Lu, C.; Yang, J.; Banger, K.; Pan, S. Methane emissions from global rice fields: Magnitude, spatiotemporal patterns, and environmental controls. *Glob. Biogeochem. Cycles* **2016**, *30*, 1246–1263. [CrossRef]
5. Carrasco, L.; Fujita, G.; Kito, K.; Miyashita, T. Historical mapping of rice fields in Japan using phenology and temporally aggregated Landsat images in Google Earth Engine. *ISPRS J. Photogramm. Remote Sens.* **2022**, *191*, 277–289. [CrossRef]
6. Xu, H.; Tian, Z.; He, X.; Wang, J.; Sun, L.; Fischer, G.; Fan, D.; Zhong, H.; Wu, W.; Pope, E.; et al. Future increases in irrigation water requirement challenge the water-food nexus in the northeast farming region of China. *Agric. Water Manag.* **2019**, *213*, 594–604. [CrossRef]
7. Chauhan, S.; Darvishzadeh, R.; Boschetti, M.; Pepe, M.; Nelson, A. Remote sensing-based crop lodging assessment: Current status and perspectives. *ISPRS J. Photogramm. Remote Sens.* **2019**, *151*, 124–140. [CrossRef]
8. Kuenzer, C.; Knauer, K. Remote sensing of rice crop areas. *Int. J. Remote Sens.* **2013**, *34*, 2101–2139. [CrossRef]
9. Weiss, M.; Jacob, F.; Duveiller, G. Remote sensing for agricultural applications: A meta-review. *Remote Sens. Environ.* **2020**, *236*, 111402. [CrossRef]
10. Xu, S.; Zhu, X.; Chen, J.; Zhu, X.; Duan, M.; Qiu, B.; Wan, L.; Tan, X.; Xu, Y.N.; Cao, R. A robust index to extract paddy fields in cloudy regions from SAR time series. *Remote Sens. Environ.* **2023**, *285*, 113374. [CrossRef]
11. Dong, J.; Xiao, X.; Kou, W.; Qin, Y.; Zhang, G.; Li, L.; Jin, C.; Zhou, Y.; Wang, J.; Biradar, C.; et al. Tracking the dynamics of paddy rice planting area in 1986–2010 through time series Landsat images and phenology-based algorithms. *Remote Sens. Environ.* **2015**, *160*, 99–113. [CrossRef]
12. Xiao, X.; Boles, S.; Liu, J.; Zhuang, D.; Frolking, S.; Li, C.; Salas, W.; Moore, B., III. Mapping paddy rice agriculture in southern China using multi-temporal MODIS images. *Remote Sens. Environ.* **2005**, *95*, 480–492. [CrossRef]
13. Xiao, X.; Boles, S.; Frolking, S.; Li, C.; Babu, J.Y.; Salas, W.; Moore, B., III. Mapping paddy rice agriculture in South and Southeast Asia using multi-temporal MODIS images. *Remote Sens. Environ.* **2006**, *100*, 95–113. [CrossRef]
14. Xiao, X.; Boles, S.; Frolking, S.; Salas, W.; Moore, B., III; Li, C.; He, L.; Zhao, R. Observation of flooding and rice transplanting of paddy rice fields at the site to landscape scales in China using VEGETATION sensor data. *Int. J. Remote Sens.* **2002**, *23*, 3009–3022. [CrossRef]
15. Ni, R.; Tian, J.; Li, X.; Yin, D.; Li, J.; Gong, H.; Zhang, J.; Zhu, L.; Wu, D. An enhanced pixel-based phenological feature for accurate paddy rice mapping with Sentinel-2 imagery in Google Earth Engine. *ISPRS J. Photogramm. Remote Sens.* **2021**, *178*, 282–296. [CrossRef]
16. Wang, M.; Wang, J.; Chen, L. Mapping paddy rice using weakly supervised long short-term memory network with time series Sentinel optical and SAR images. *Agriculture* **2020**, *10*, 483. [CrossRef]
17. Zhang, X.; Wu, B.; Ponce-Campos, G.E.; Zhang, M.; Chang, S.; Tian, F. Mapping up-to-date paddy rice extent at 10 m resolution in china through the integration of optical and synthetic aperture radar images. *Remote Sens.* **2018**, *10*, 1200. [CrossRef]
18. Bazzi, H.; Baghdadi, N.; El Hajj, M.; Zribi, M.; Minh, D.H.T.; Ndikumana, E.; Courault, D.; Belhouchette, H. Mapping paddy rice using Sentinel-1 SAR time series in Camargue, France. *Remote Sens.* **2019**, *11*, 887. [CrossRef]
19. Li, H.; Fu, D.; Huang, C.; Su, F.; Liu, Q.; Liu, G.; Wu, S. An approach to high-resolution rice paddy mapping using time-series Sentinel-1 SAR data in the Mun River Basin, Thailand. *Remote Sens.* **2020**, *12*, 3959. [CrossRef]
20. Tian, H.; Wu, M.; Wang, L.; Niu, Z. Mapping early, middle and late rice extent using sentinel-1A and Landsat-8 data in the poyang lake plain, China. *Sensors* **2018**, *18*, 185. [CrossRef]
21. Gao, Y.; Pan, Y.; Zhu, X.; Li, L.; Ren, S.; Zhao, C.; Zheng, X. FARM: A fully automated rice mapping framework combining Sentinel-1 SAR and Sentinel-2 multi-temporal imagery. *Comput. Electron. Agric.* **2023**, *213*, 108262. [CrossRef]
22. Zhan, P.; Zhu, W.; Li, N. An automated rice mapping method based on flooding signals in synthetic aperture radar time series. *Remote Sens. Environ.* **2021**, *252*, 112112. [CrossRef]
23. Karimi, N.; Taban, M.R. A convex variational method for super resolution of SAR image with speckle noise. *Signal Process. Image Commun.* **2021**, *90*, 116061. [CrossRef]
24. Klogo, G.S.; Gasonoo, A.; Ampomah, I.K. On the performance of filters for reduction of speckle noise in SAR images off the coast of the Gulf of Guinea. *arXiv* **2013**, arXiv:1312.2383. [CrossRef]
25. Han, J.; Zhang, Z.; Luo, Y.; Cao, J.; Zhang, L.; Cheng, F.; Zhuang, H.; Zhang, J.; Tao, F. AsiaRiceMap10m: High-resolution annual paddy rice maps for Southeast and Northeast Asia from 2017 to 2019. *Earth Syst. Sci. Data Discuss.* **2021**, *2021*, 5969–5986. [CrossRef]
26. He, Y.; Dong, J.; Liao, X.; Sun, L.; Wang, Z.; You, N.; Li, Z.; Fu, P. Examining rice distribution and cropping intensity in a mixed single-and double-cropping region in South China using all available Sentinel 1/2 images. *Int. J. Appl. Earth Obs. Geoinf.* **2021**, *101*, 102351. [CrossRef]
27. Mansaray, L.R.; Wang, F.; Huang, J.; Yang, L.; Kanu, A.S. Accuracies of support vector machine and random forest in rice mapping with Sentinel-1A, Landsat-8 and Sentinel-2A datasets. *Geocarto Int.* **2020**, *35*, 1088–1108. [CrossRef]

28. Park, S.; Im, J.; Park, S.; Yoo, C.; Han, H.; Rhee, J. Classification and mapping of paddy rice by combining Landsat and SAR time series data. *Remote Sens.* **2018**, *10*, 447. [CrossRef]
29. Singha, M.; Dong, J.; Zhang, G.; Xiao, X. High resolution paddy rice maps in cloud-prone Bangladesh and Northeast India using Sentinel-1 data. *Sci. Data* **2019**, *6*, 26. [CrossRef]
30. Zhao, X.; Nishina, K.; Akitsu, T.K.; Jiang, L.; Masutomi, Y.; Nasahara, K.N. Feature-based algorithm for large-scale rice phenology detection based on satellite images. *Agric. For. Meteorol.* **2023**, *329*, 109283. [CrossRef]
31. Thorp, K.; Drajat, D. Deep machine learning with Sentinel satellite data to map paddy rice production stages across West Java, Indonesia. *Remote Sens. Environ.* **2021**, *265*, 112679. [CrossRef]
32. Torbick, N.; Chowdhury, D.; Salas, W.; Qi, J. Monitoring rice agriculture across myanmar using time series Sentinel-1 assisted by Landsat-8 and PALSAR-2. *Remote Sens.* **2017**, *9*, 119. [CrossRef]
33. Chen, N.; Yu, L.; Zhang, X.; Shen, Y.; Zeng, L.; Hu, Q.; Niyogi, D. Mapping paddy rice fields by combining multi-temporal vegetation index and synthetic aperture radar remote sensing data using google earth engine machine learning platform. *Remote Sens.* **2020**, *12*, 2992. [CrossRef]
34. Valero, S.; Morin, D.; Inglada, J.; Sepulcre, G.; Arias, M.; Hagolle, O.; Dedieu, G.; Bontemps, S.; Defourny, P.; Koetz, B. Production of a dynamic cropland mask by processing remote sensing image series at high temporal and spatial resolutions. *Remote Sens.* **2016**, *8*, 55. [CrossRef]
35. Millard, K.; Richardson, M. On the importance of training data sample selection in random forest image classification: A case study in peatland ecosystem mapping. *Remote Sens.* **2015**, *7*, 8489–8515. [CrossRef]
36. Boryan, C.; Yang, Z.; Mueller, R.; Craig, M. Monitoring US agriculture: The US department of agriculture, national agricultural statistics service, cropland data layer program. *Geocarto Int.* **2011**, *26*, 341–358. [CrossRef]
37. Shen, R.; Pan, B.; Peng, Q.; Dong, J.; Chen, X.; Zhang, X.; Ye, T.; Huang, J.; Yuan, W. High-resolution distribution maps of single-season rice in China from 2017 to 2022. *Earth Syst. Sci. Data Discuss.* **2023**, *2023*, 1–27. [CrossRef]
38. Pan, B.; Zheng, Y.; Shen, R.; Ye, T.; Zhao, W.; Dong, J.; Ma, H.; Yuan, W. High resolution distribution dataset of double-season paddy rice in China. *Remote. Sens.* **2021**, *13*, 4609. [CrossRef]
39. Wang, L.; Ma, H.; Li, J.; Gao, Y.; Fan, L.; Yang, Z.; Yang, Y.; Wang, C. An automated extraction of small-and middle-sized rice fields under complex terrain based on SAR time series: A case study of Chongqing. *Comput. Electron. Agric.* **2022**, *200*, 107232. [CrossRef]
40. He, Z.; Li, S.; Wang, Y.; Dai, L.; Lin, S. Monitoring rice phenology based on backscattering characteristics of multi-temporal RADARSAT-2 datasets. *Remote Sens.* **2018**, *10*, 340. [CrossRef]
41. He, Z.; Li, S.; Chang, M.; Liu, Y.; Liu, K.; Wan, L.; Wang, Y. Novel harmonic-based scheme for mapping rice-crop intensity at a large scale using time series Sentinel-1 and ERA5-Land datasets. *IEEE Trans. Geosci. Remote Sens.* **2024**, *62*, 4406523. [CrossRef]
42. Guan, K.; Li, Z.; Rao, L.N.; Gao, F.; Xie, D.; Hien, N.T.; Zeng, Z. Mapping paddy rice area and yields over thai binh province in viet nam from modis, landsat, and alos-2/palsar-2. *IEEE J. Sel. Top. Appl. Earth Obs. Remote Sens.* **2018**, *11*, 2238–2252. [CrossRef]
43. Xiao, W.; Xu, S.; He, T. Mapping paddy rice with sentinel-1/2 and phenology-, object-based algorithm—A implementation in Hangjiahu plain in China using gee platform. *Remote Sens.* **2021**, *13*, 990. [CrossRef]

Disclaimer/Publisher's Note: The statements, opinions and data contained in all publications are solely those of the individual author(s) and contributor(s) and not of MDPI and/or the editor(s). MDPI and/or the editor(s) disclaim responsibility for any injury to people or property resulting from any ideas, methods, instructions or products referred to in the content.